Research Square

Preprints are preliminary reports that have not undergone peer review.
They should not be considered conclusive, used to inform clinical practice,
or referenced by the media as validated information.

Fe/Cu Bimetallic Particles for TCAL Dechlorination: From Parameter Effects to Reusable Catalysis with Mechanistic Insights

Runlong Chen
Chinese Research Academy of Environmental Sciences
Jie Wang
wangjie_hj@tongji.edu.cn

Chinese Research Academy of Environmental Sciences
Lianhua Yuan
Chinese Research Academy of Environmental Sciences
Zhiqiang Shen
Chinese Research Academy of Environmental Sciences
Yuexi Zhou
Chinese Research Academy of Environmental Sciences
Yanyue Gu
Chinese Research Academy of Environmental Sciences
Xuwen He
China University of Mining and Technology

Research Article

Keywords: Fe/Cu bimetallic particles, TCAL, Dechlorinate, Reaction Mechanisms, Reusability Assessment

Posted Date: March 10th, 2026

DOI: https://doi.org/10.21203/rs.3.rs-8519496/v1

License: This work is licensed under a Creative Commons Attribution 4.0 International License.
Read Full License

Additional Declarations: No competing interests reported.

Abstract

Iron/copper (Fe/Cu) bimetallic particles have demonstrated high activity for the dechlorination of trichloroacetaldehyde (TCAL). To enhance the dechlorination efficacy, a systematic evaluation of key operational parameters—such as chelator concentration, bimetal dosage, copper loading, and initial pH—is essential. The Fe/Cu bimetallic composites were synthesized and applied under optimized conditions (25 g/L Fe/Cu, EDTA/Cu molar ratio of 1:10, 1% Cu loading, initial pH 8). The materials were characterized before and after reaction using SEM-EDS, XRD, and XPS. Reaction intermediates were analyzed by gas chromatography with a micro electron capture detector (GC-μECD) to propose a degradation pathway. Under optimal conditions, a high TCAL removal rate of 98.18% and a dechlorination efficiency of 38.70% were achieved within 48 hours. Material characterization confirmed an iron-core structure with surface-deposited copper, which facilitated synergistic galvanic corrosion and improved surface reactivity. The degradation was attributed to hydrogen radicals (H•), the reducing power of Fe^0 and Fe^{2+}, and the adsorption by iron oxides (Fe_2O_3 and FeOOH). The Fe/Cu catalyst exhibited excellent recyclability over five cycles, and the degradation kinetics followed a pseudo-first-order model.

1. Introduction

Chloroacetaldehydes (CALs) encompasses three chlorinated derivatives: trichloroacetaldehyde (TCAL), dichloroacetaldehyde (DCAL), and chloroacetaldehyde (CAL). The generation of wastewater containing CALs has been increasing due to the growing production of CALs in chemical plants (Bommer et al., 2014). CALs are also produced during water treatment using chlorine disinfection (Huang et al., 2021; Hua et al., 2021). Due to its relatively stable structure, TCAL is less susceptible to chemical and biological degradation within CALs (Tian et al., 2020). The presence of aldehyde groups and more chlorine atoms contributes to the higher toxicity of TCAL compared to DCAL and CAL (Tian et al., 2021). TCAL has the potential to cause teratogenicity (Procházka, et al., 2019), carcinogenicity (Richardson et al., 2007), and mutagenicity (Huang, et al., 2021). The International Agency for Research on Cancer (IARC) designated TCAL as a Group 2A carcinogen. This chlorinated aldehyde demonstrates bioaccumulation potential through aquatic food chains and water supplies (Yu et al., 2020).

Zero-valent iron (ZVI) has low redox potential (E_0= -0.44 V), as an electron donor, transferring electrons to halogenated organic compounds, enabling dechlorination (Gao et al. 2015; Zhao et al. 2016). Furthermore, Fe^{2+} formed after the corrosion of ZVI can also facilitate the reduction and detoxification of chlorinated organic compounds (Fan et al. 2023). While ZVI has demonstrated effectiveness in groundwater remediation and wastewater treatment for organic pollutants (Fu et al.,2014), particularly in degrading diverse chlorinated compounds (Song and Carraway, 2005), its practical application faces limitations. Surface passivation caused by iron hydroxide precipitation significantly reduces reactive site availability, thereby impeding contaminant-ZVI interfacial interactions (Bae et al., 2018;). To overcome this limitation and enhance ZVI reactivity, a second catalytic metal is often introduced to form a

bimetallic system. Such bimetallic composites exhibit improved reaction kinetics and higher overall activity in the removal of diverse pollutants compared to ZVI alone.

Catalytic dechlorination systems employing bimetallic couples offer an eco-efficient strategy for mineralization of persistent chloroorganic compounds (Yamaguchi et al., 2018; Choi et al., 2008). Researchers have enhanced the reduction efficiency of ZVI by planting catalytic metals on the ZVI to prepare bimetals. Bimetallic systems operate through two functional components: (1) Active metals (Fe,Al,Mg,Zn,Sn) serving as electron donors for H_2 generation; (2) Catalytic metals (Pd,Pt,Cu,Ni) enhancing dechlorination via H_2 utilization and accelerated substrate corrosion through anode-cathode galvanic interactions (Ji et al., 2022; Han et al., 2019). Adding other metals with ZVI can to some extent overcome the drawbacks associated with dichlorination (Guo et al., 2021), enhancing the dechlorination rate. Fe/Cu bimetallic particles have been found to effectively reduce and degrade Acid Orange 7(AO_7) (Yuan et al., 2014), trichloroethylene(TCE) (He et al., 2018), nitrates (Zeng et al., 2017), and sulfamethoxazole (SMT) (Dong et al., 2022). Relative to ZVI, the Fe/Cu bimetallic system exhibits superior pollutant removal efficiency through improved reaction rates and catalytic performance. EDTA is a widely used chelating agent, and bimetallic materials can be prepared using EDTA to form complexes with metal ions through its multiple coordination sites (Zhou et al., 2023). Bimetals such as Ag/Au (Shevchenko et al., 2019), Al/Cu (Wei et al., 2022), and Fe/Mn-N (Song et al., 2022) have been synthesized using EDTA as a chelating agent, indicating that using EDTA to synthesize Fe/Cu bimetallic particles is a potential method. However, the degradation of TCAL by bimetallic nanoparticles has not been reported, and the mechanism by which bimetallic nanoparticles degrade TCAL remains unclear. Therefore, elucidating the operative pathways of TCAL degradation via bimetallic nanocomposites remains critical for advancing catalytic remediation technologies.

The study utilized EDTA to prepare Fe/Cu bimetallic particles. Parametric optimization encompassed both Fe/Cu particle synthesis variables and operational parameters affecting TCAL dechlorination performance. Characterization was conducted before and after the use of the bimetallic system, and the dechlorination products of TCAL were determined. The research elucidated the dechlorination mechanisms of Fe/Cu bimetallic particles toward TCAL degradation while assessing the material's regenerative capacity through multiple reuse cycles.

2. Experimental

2.1. Materials and reagents

All reagents were procured at analytical-grade purity (≥ 99.0%). Analytical-grade copper and 100-mesh zero-valent iron (ZVI) were utilized for both Fe/Cu bimetal fabrication and parallel control experiments.

2.2. Preparation of Fe/Cu bimetallic particles

In this study, a solution-phase synthetic route was utilized for the controlled preparation of Fe/Cu bimetallic particulate systems. The reduced iron powder was immersed in 0.05 mol/L H_2SO_4 for 10

minutes, then thoroughly rinsed with ultrapure water until achieving pH 7.0. Subsequently, the powder was placed in a beaker for later use. A 200 mL copper sulfate solution, along with ethylenediaminetetraacetic acid disodium (EDTA-2Na) as a chelating agent, was added to the beaker, and then mixed with the pretreated reduced iron powder. The mixture was shaken for 15 minutes in a constant-temperature shaker incubator at a rotation speed of 250 rpm. Remove Fe/Cu from the incubator and stand for 5 min. The prepared Fe/Cu was rinsed with pure water three times, underwent an anhydrous ethanol rinse cycle followed by 40-minute nitrogen-protected desiccation at 80°C.

2.3. TCAL removal experiments

A 100 mg/L TCAL solution (200 mL) was transferred into a 250 mL conical flask for reaction. Fe/Cu bimetal catalysts (5 g total mass, 1% Cu by mass) were introduced into the reaction medium. System pH was regulated through titration with 0.1 M H_2SO_4 and 0.1 M NaOH solutions. To improve the electrical conductivity of the system, 3 mL of 0.05% Na_2SO_4 solution was added. After 3 minutes of nitrogen blowing, the flask was sealed with parafilm and placed in a temperature-controlled shaker, set at 25°C and a rotation speed of 200 rpm. Sampling was carried out using a syringe at different time intervals, and the concentrations of TCAL and chloride ions were determined.

2.4. Analytical methods

2.4.1. SEM and EDS

The specific test conditions included a working voltage of 5 kV and a resolution of 1.3 nm.

2.4.2. XRD and XPS

The XRD (Bruker D8, Germany) profiles were obtained using a Cu-Kα radiation source at 36 kV with a scanning rate of 2°/min and a scanning range of 10 to 90°. After analyzing the XRD patterns, the composition was compared with the standard PDF cards.

The experiment employed an X-ray photoelectron spectrometer (Thermo Scientific K-Alpha$^+$) to test the prepared Fe/Cu materials. The XPS analysis chamber's vacuum degree is better than 5×10^{-9} mbar, with a voltage of 15 KV and a beam current of 15 mA. A monochromatic Al Kα source is utilized as the X-ray source, with an X-ray beam spot size of 400 μm. For the full spectrum, the energy range is 150 eV, and the step size is 1.0 eV, while in the narrow spectrum, the energy is 50 eV, and the step size is 0.1 eV. The analysis results were fitted using XPSPEAK software.

2.4.3. *Determination of TCAL and chloride ion concentration*

The concentration of TCAL was determined using spectrophotometry. A suitable volume of the water sample (1 mL to 5 mL) was mixed with 5 mL of phosphate buffer solution in a 25 mL colorimetric tube. After shaking, 5 mL of 0.5% zylophenone color developer solution was added, followed by the addition of distilled water to the marking line. The mixture was then heated in a water bath at 80 ± 2°C for 40

minutes after shaking, cooled to 25°C, and its absorbance at 480 nm was measured using a 10 mm cuvette, with the blank solution serving as a reference. The concentration of TCAL was determined using the standard curve obtained.

The concentration of chloride was analyzed using ion chromatography. During the determination, 5 mL of the supernatant was passed through a 0.45 μm membrane and then injected into an ion chromatograph. The specific test conditions were as follows: anion-exchange column AS11-HC, 4 × 250 mm, anion-protecting column IonPacAS11HC, 50 mm×4 mm, column temperature 35℃, inhibitory current 75 mA, flow rate 1 mL/min.

2.4.4. *Determination of Degradation Products of Trichloroacetaldehyde*

The analytical method for chloral hydrate determination is adapted from EPA Method 551.1. A 5 mL water sample was extracted with 3 mL of methyl tert-butyl ether in the presence of 1 g anhydrous sodium sulfate, vortexed for 1 min, and allowed to separate. The organic layer was analyzed by GC-μECD (Agilent, USA) using a DB-5 column (30 m × 0.32 mm × 0.25 μm) with high-purity nitrogen as the carrier gas. The oven temperature was programmed from 45°C (hold 4 min) to 55°C at 15°C/min (hold 5 min), then to 65°C at 15°C/min (hold 3 min), to 150°C at 30°C/min (hold 3 min), and finally to 250°C at 20°C/min (hold 2 min). The injector and detector temperatures were 250°C and 240°C, respectively, with a split ratio of 8:1. The carrier gas flow was programmed from 0.5 mL/min (hold 11.33 min) to 1.0 mL/min (hold 4 min) and then to 2.0 mL/min (hold 3 min), with a constant makeup gas flow of 50 mL/min.

3. Results and discussion

3.1. Removal rate and dechlorination rate of TCAL by Fe/Cu bimetallic particles

3.1.1. *Effect of different chelating doses*

Fe/Cu bimetallic particles with different molar ratios of EDTA/Cu were prepared. The variations in removal efficiency and dechlorination of TCAL under different chelating agent proportions in Fe/Cu bimetallic particles are presented in Fig. 1a **and b**. The removal rate and dechlorination rate of TCAL were similar. Both increased rapidly within 12 h, and then slowed down until it stabilized. As the EDTA/Cu molar ratio increased from 0 to 1:10, the TCAL removal rate rose from 96.76% to 98.18%, and the dechlorination rate improved from 30.79% to 38.79% at 48 h. However, further increasing the EDTA/Cu ratio to 1:1 reduced the TCAL removal rate to 94.43% and significantly lowered the dechlorination rate to 28.84%.

The dispersing effect of chelating agent can effectively reduce the aggregation of Cu, making Cu uniformly distributed and form more catalytic sites (Shevchenko et al., 2019). When the EDTA was insufficient, Cu was in an aggregated state, unevenly distributed on the ZVI surface, resulting in a small reaction area (Ren and Lai, 2016). When the concentration of EDTA is too high, a dense Cu coating is formed at the ZVI interface, which greatly reduces the active sites on the Fe surface (Chen et al., 2018). Yang, B et al. (Yang et al., 2014) and Liu et al. (Liu et al., 2015) both used EDTA-4Na to prepare bimetals for the removal of chlorinated organics and reached similar conclusions. Considering the removal and dechlorination rates, the most efficient removal of Fe/Cu bimetallic particles was achieved when EDTA/Cu = 1:10.

3.1.2. *Effect of theoretical copper loading*

The study prepared five Fe/Cu formulations with incremental copper contents: 0% (control), 0.5%, 1%, 2%, and 3% by mass. The variations in removal efficiency and dechlorination rate of TCAL under different Cu loadings in Fe/Cu bimetallic particles are presented in Fig. 1c **and d**. The removal efficiency and dechlorination of TCAL both increase correspondingly within the first 12 h and eventually reaching a stable state. When the theoretical copper loading is 0 (ZVI), the efficiency is significantly lower compared to the Fe/Cu bimetallic particles. The Fe/Cu bimetallic particles with copper loadings of 0.5%, 1%, 2%, and 3% achieved removal rates of 96.64%, 98.18%, 96.58%, and 96.52% for TCAL after 48 h, with dechlorination rates of 33.03%, 38.70%, 30.73%, and 31.44%, respectively. The Fe/Cu bimetallic particles with a 1% copper loading demonstrated the most optimal performance compared to other copper loadings.

The promotion effect on the dechlorination of TCAL can be attributed to two main factors: reductive effect of ZVI and galvanic cell effect of the bimetallic system (Yang et al., 2021; Peng et al., 2020). An excessively high copper loading reduces the contact between TCAL and ZVI, weakening the catalytic reduction effect on TCAL (Chen et al., 2018). When the copper loading is low, it is not sufficient to induce changes in the surface properties of ZVI, and a galvanic cell cannot be formed. Both excessively high and excessively low copper loadings are detrimental to dechlorination. These findings align reported 2,4-DCP removal efficiencies using analogous Fe/Cu bimetallic systems (Pan et al., 2019).

3.1.3. *Effect of Fe/Cu bimetal dosage*

Figure 1e **and f** demonstrate the TCAL removal efficiency variations corresponding to different Cu loadings in Fe/Cu bimetallic composites. It can be observed that with an increase in the dosage, both the removal rate and dechlorination efficiency of TCAL initially increased and then stabilized. At 48 h, the corresponding removal rates are 92.77%, 95.68%, 98.18%, 98.12%, 98.72%, and 98.84%, with dechlorination rates of 27.08%, 27.85%, 38.70%, 39.02%, 39.56%, and 40.51%, respectively.

The results showed that increasing the amount of Fe/Cu bimetallic particles improved TCAL dechlorination. Increased bimetallic particle dosage enhances reactive site availability, thereby improving contaminant degradation capacity (Yamaguchi et al., 2018). This is the same as the results obtained

using Pd/Fe bimetallic particles to remove pentachlorobiphenyl (He et al., 2009). Considering removal rate, dechlorination and economics, 25 g/L Fe/Cu particles showed optimal performance.

3.1.4. *Effect of initial pH*

Figure 1g **and h** present the effects of initial pH values on both TCAL removal and dechlorination efficiencies using Fe/Cu bimetallic particles. At 3 h, the removal rates of TCAL for the Fe/Cu bimetallic system with initial pH values of 3, 4, 5, 6, 7, 8, and 9 were 82.16%, 81.59%, 80.1%, 81.99%, 73.66%, 79.91%, and 75.74% with dechlorination rates of 16.71%, 15.98%, 16.66%, 16.45%, 18.67%, 33.81%, and 15.99%, respectively. At 48 h, the corresponding removal rates at different pH levels reached 96.76%, 97.35%, 97.83%, 97.89%, 98.01%, 98.18%, and 96.64%, with dechlorination rates of 23.44%, 23.74%, 25.33%, 26.42%, 28.28%, 38.70%, and 23.33%, respectively. At 3 h, acidic conditions were more favorable for TCAL removal and dechlorination. However, in the subsequent reactions, the effect under high pH conditions was more effective. The results above demonstrate that at an initial pH of 8, the catalytic reduction of TCAL by Fe/Cu bimetallic particles is more effective. Zhang, W et al. also suggested that it is best under neutral conditions (Zhang et al., 2013).

Research demonstrates that the primary reduction pathway for pollutants in the Fe/Cu bimetallic system is direct electron transfer on the copper surface. Under neutral conditions, particle corrosion results in the deposition of iron (oxyhydr)oxides, a process wherein these deposits form highly reactive sites(Sun et al., 2016). The adsorption and concentration of reactants at these sites significantly promote the reduction reaction and accelerate the desorption of degradation products. Acidic conditions promote Fe/Cu particle corrosion, thereby increasing ZVI-derived H• generation (Zhu et al., 2012). The generated H• subsequently facilitates the reduction of TCAL. Consequently, the catalytic reduction efficiency of TCAL is improved in the initial stages under acidic condition (He et al., 2018). As the pH increases further, the corrosion rate of Fe/Cu bimetallic particles significantly decreases (Yamaguchi et al., 2018; Ji et al., 2017), leading to a substantial reduction in the generation rate of H• and metal oxides, which in turn diminishes the reaction activity.

3.2. Mechanism analysis of Fe/Cu bimetal removal of TCAL

3.2.1. *Characterization of Fe/Cu bimetal*

Figure 2 presents the SEM-EDS characterization of Fe/Cu bimetallic particles. The original figure can be found in Figure S1. Figure 2a-d demonstrates that the Fe/Cu bimetallic particles consisted primarily of Cu and Fe. With the EDTA/Cu molar ratio incrementally raised from 0 to 1:10, effect of Cu planting was superior. However, when the ratio further increased to 1:1, Cu exhibited significant enrichment, reducing the active sites. The optimal ratio of EDTA to Cu is 1:10, consistent with previous experimental results. After TCAL reduction and dechlorination by Fe/Cu (Fig. 2e), irregular block-shaped protrusions were observed on the surface. These protrusions occupy the active sites and severely impede the reduction and dechlorination process. Additionally, oxygen was detected on the Fe/Cu bimetallic particles, suggesting passivation of the Fe/Cu surface after the use.

The study conducted XRD analysis to determine the composition of the Fe/Cu bimetallic particles (Fig. S3). By comparing with standard PDF cards, the diffraction peaks at 2θ = 44.7°, 2θ = 65.05°, and 2θ = 82.37° were identified as characteristic peaks of Fe with no detectable peaks related to iron oxides or other impurities, indicating that Fe/Cu bimetallic particles were prepared without impurities. The characteristic peak of Cu is not observed in the spectrum, primarily due to the good dispersibility and low loading content of Cu. Post-reaction XRD analysis revealed no significant phase changes in the Fe/Cu bimetallic material, indicating structural reusability of Fe/Cu particles during the reaction.

The surface chemical states of Fe/Cu particles were examined by XPS before and after reaction (Fig. 3). Figure 3a displays three characteristic peaks for the Fe/Cu bimetallic particles: Fe2p, Cu2p, and O1s. The continuous presence of the Cu peak before and after the use suggests that Cu, in the process of catalytic reduction of TCAL by Fe/Cu, serves as a protected anode, primarily playing a catalytic and passivating role. The characteristic peaks of Fe2p at binding energies of 712.2 eV and 725.8 eV correspond to Fe_2O_3, and peaks at 713.8 eV and 727.0 eV correspond to FeOOH. Figure 3b conclusively demonstrates the presence of Fe_2O_3 and FeOOH phases within the surface oxide matrix of Fe/Cu compositesm consistent with the results previously reported (Pan et al., 2023). This suggests that surface passivation occurs on Fe/Cu.

3.2.2. *Analysis of reaction products*

To elucidate the Fe/Cu reduction mechanism of TCAL, the concentrations of Cu^{2+}, Fe^{2+}, and Fe^{3+} were quantitatively determined using an atomic absorption spectrophotometer (AA-6300, China) and the o-phenanthroline spectrophotometric method, respectively. After the reaction, no copper ions were detected in the Fe/Cu bimetallic system, indicating that copper plays a catalytic role in the process of catalytic reduction of TCAL by Fe/Cu, enhancing the reaction rate without being consumed. XPS characterization provided corroborating evidence for these observations (Fig. 3).

The concentrations of Fe^{2+} and Fe^{3+} were determined (Fig. 4). In both the ZVI and Fe/Cu systems, the trend of Fe^{2+} showed an initial increase followed by a subsequent decrease, while the Fe^{3+} concentration increased overall over the reaction time. In the Fe/Cu bimetallic system, the Fe^{2+} concentration increased to 245.71 mg/L within 12 h, then decreased to 227.01 mg/L at 96 h, and the Fe^{3+} concentration continued to increase to 36.71 mg/L at 96 h. In the ZVI system, the Fe^{2+} concentration reached its maximum value of 234.49 mg/L at 48 h, subsequently decreasing to 222.03 mg/L at 96 h. The Fe^{3+} concentration reached 65.39 mg/L at 96 h, which is 1.78 times higher than that in the Fe/Cu bimetallic system.

The primary driving force behind the reduction and dechlorination of TCAL by ZVI is predominantly attributed to the oxidation process of Fe (Ruan et al., 2020). During the initial phase of the reaction, Fe undergoes rapid oxidation to form Fe^{2+}, leading to a rapid increase in Fe^{2+} concentration. As the reaction progresses, the formation of a passivation film impedes the oxidation process of Fe (Li et al., 2020), resulting in a gradual decrease in generated Fe^{2+} and subsequently diminishing dechlorination effects.

Concurrently, Fe^{2+} is oxidized to form Fe^{3+}, providing electrons for TCAL to facilitate its reduction and dichlorination (Ruan et al., 2019), while continuously being consumed. Furthermore, both the concentration and dissolution rate of Fe^{2+} in Fe/Cu bimetallic system exceed those in ZVI system, whereas both concentration and dissolution rate of Fe^{3+} are lower than those found in ZVI system. This indicates that Fe/Cu bimetallic system exerts a more pronounced effect on promoting reduction and dechlorination processes associated with TCAL.

Qualitative analysis by GC-μECD was conducted across different initial TCAL concentrations at 6 and 96 h reaction time (Fig. 5). It is evident that Fe/Cu can effectively remove concentrations of TCAL within 6 h. The primary product at 6 h is DCAL (peak time at 7.430 min). At 96 h, the predominant dechlorination products of TCAL are DCAL and CAL (peak time at 6.577 min), as well as a minor amount of chloroethanol (ECH, peak time at 14.233 min). These findings suggest that TCAL initially undergoes single chlorine atom removal to form DCAL, followed by subsequent elimination of another chlorine atom to generate CAL. Furthermore, as the reaction advances, a portion of CAL's aldehyde group is further reduced to yield the corresponding alcohol group, resulting in ECH production (Sarma and Goswami, 2009). Zhou et al. utilized $Zn/CdSO_4$ and $Zn/SnCl_2$ bimetallic systems involving aldehydes or ketones and achieved substantial propenyl alcohol formation (Zhou et al., 2004). These results underscore the capability of bimetallic systems in reducing aldehyde to alcohol. Based on the GC-μECD results, the reaction equation for the reduction and degradation of TCAL by TCL was obtained (Text S2).

3.2.3. *Reaction mechanism*

The TCAL removal can be attributed to three mechanisms (Fig. 6). First, The Fe/Cu system facilitates the creation of abundant micro-galvanic cells. Under the effect of galvanic cells, a potential difference accelerates the corrosion of ZVI in Fe/Cu, producing H•. The generated H• can dechlorinate TCAL, yielding DCAL. CAL and CA can be generated in the same way. Secondly, Fe and Fe^{2+} in the system are oxidized to Fe^{2+} and Fe^{3+}, providing electrons which can also facilitate the gradual dechlorination of TCAL (Zhu et al., 2010). Thirdly, the metal oxides such as Fe_2O_3 and FeOOH adsorb some TCAL. This is also the reason for the high TCAL removal rate and low dechlorination rate during the previous experiments.

3.3. Fe/Cu reuse potential study

The reaction rate constant can provide a more intuitive description of the difference in the reaction rates of the reduction of TCAL catalyzed by Fe/Cu and ZVI. After the use of Fe/Cu, rinse with distilled water and dry with nitrogen gas for further use. After continuous use of Fe/Cu for five cycles, the removal rate of TCAL decreased from 98.07% to 96.34% within 24 h, representing a decrease of just 1.73%. In contrast, the removal rate of TCAL by ZVI decreased from 76.70% to 63.96%, a decrease of 12.74%. Compared to ZVI, Fe/Cu presents a better potential for reusability (Li et al., 2018).

With the repeated use of Fe/Cu, part of ZVI is oxidized to Fe^{2+} and Fe^{3+} and dispersed into the solution, resulting in a change in the original structure and a reduction in the number of competing pairs

(Yamaguchi et al., 2018). There are also Fe_2O_3 and FeOOH, deposited on the surface of the bimetal (Ji et al., 2017). In addition, alkaline environment and electrochemical reaction conditions destroy the cross-linking bond of chelating agent, causing irreversible loss of Fe/Cu (Yang et al., 2014; Fan et al., 2015).

Figure S2 presents the fitted TCAL removal efficiency data for Fe/Cu and ZVI during multiple cycles. Kinetic fitting results of Fe/Cu and ZVI to TCAL removal process are shown in Table S1 and Table S2. The results show that TCAL degradation by Fe/Cu and ZVI over five cycles follows pseudo-first-order kinetics (R^2>0.93). A negative correlation exists between reuse cycle number and apparent rate constants for TCAL removal by Fe/Cu and ZVI.

The reusability of Fe/Cu and ZVI in removing TCAL over multiple cycles is shown in Fig. 7. As the number of uses increases, the apparent rate constant for the catalytic reduction (k_{obs}) of TCAL by Fe/Cu gradually decreases from 0.11 h^{-1} to 0.096 h^{-1}, indicating a gradual decrease in the self-oxidation ability of Fe/Cu with continued use. It is noteworthy that after the fifth cycle, the apparent rate constant of TCAL removal by Fe/Cu remains 2.7 times that of ZVI for the same number of uses, and it is 1.79 times that of ZVI after the first use. This indicates that Cu loading on the surface of ZVI enhances its reactivity in TCAL removal, effectively preventing the passivation of Fe/Cu and promoting the reduction and dechlorination of TCAL and the recyclability of Fe/Cu.

4. Conclusion

Fe/Cu bimetallic particles synthesized with EDTA remarkably effective TCAL removal capability. Under the optimum conditions (Fe/Cu dosage: 25 g/L, initial pH: 8, EDTA/Cu molar ratio: 1:10, copper loading: 1 wt%), a TCAL removal efficiency of 98.18% with a dechlorination efficiency of 38.70% was achieved. The material characterization results confirm that the Fe/Cu composite material has formed an ideal structure with iron as the core and copper deposited on the surface. This structure, through the synergistic effect of the galvanic cell effect, significantly enhances the surface reactivity and corrosion resistance of the material. The oxides/hydroxides such as Fe_2O_3 and FeOOH formed on the material surface undergo adsorption. Based on the analysis of intermediate products, we proposed a possible degradation pathway of TCAL, and the removal mechanism mainly attributed to the H• generated by the galvanic cell corrosion, the reduction effect of ZVI and Fe^{2+}, and the adsorption of metal hydroxides. TCAL degradation kinetics followed pseudo-first-order reaction patterns under bimetal catalysis. This provides important reliability and economic basis for its application in actual environmental remediation projects. Furthermore, the Fe/Cu bimetallic particles exhibited exceptional recyclability, maintaining stable dechlorination performance over five consecutive reaction cycles, underscoring their potential for practical application. In conclusion, this study not only provides an efficient and reusable Fe/Cu bimetallic catalytic system for the governance of TCAL, but also deepens the understanding of the synergistic effect of reduction and adsorption in the bimetallic system at the mechanism level.

Declarations

Funding

This work was financially supported by the Central Financial Science and Technology Plan (2021-JY-32), the National Natural Science Foundation of China (No. 51508538), National Water Pollution Control and Treatment Science and Technology Major Project of China (No. 2017ZX07402002).

Author Contributions

Runlong Chen: Writing-Original Draft, Validation, Visualization, Formal analysis.

Lianhua Yuan: Data curation, Software, Formal analysis, Investigation.

Jie Wang: Data curation, Formal analysis, Writing-Review & Editing.

Zhiqiang Shen: Methodology, Writing-Review & Editing, Funding acquisition, Resources.

Yuexi Zhou: Project administration, Resources, Funding acquisition.

Yanyue Gu: Data Curation, Writing-Review &Editing.

Xuwen He: Resources Visualization.

Ethics Approval and Consent to Participate Not applicable.

Consent for Publication Not applicable.

Competing interest The authors declare no competing interests.

Availability of data and materials The raw data supporting the conclusions of this article will be made available by the authors on request.

References

1. Bae, S., Collins, R.N., Waite, T.D., Hanna, K., 2018. Advances in Surface Passivation of Nanoscale Zerovalent Iron: A Critical Review. Environ. Sci. Technol. 52,12010-12025. https://doi.org/10.1021/acs.est.8b01734.
2. Bommer, M., Kunze, C., Fesseler, J., Schubert, T., Diekert, G., Dobbek, H., 2014. Structural basis for organohalide respiration. Science. 346,455-458. https://doi.org/10.1126/science.1258118.
3. Chen, S.H., Chu, W.H., Wei, H.B., Zhao, H.Y., Xu, B., Gao, N.Y., Yin, D.Q., 2018. Reductive dechlorination of haloacetamides in drinking water by Cu/Fe bimetal. Sep. Purif. Technol. 203, 226-232. https://doi.org/10.1016/j.seppur.2018.04.048.
4. Choi, H., Al-Abed, S.R., Agarwal, S., Dionysiou, D.D., 2008. Synthesis of reactive nano-Fe/Pd bimetallic system-impregnated activated carbon for the simultaneous adsorption and dechlorination of PCBs. Chem. Mater. 20, 3649-3655. https://doi.org/10.1021/cm8003613.

5. Dong, Q.X., Dong, H.R., Li, Y.J., Xiao, J.Y., Xiang, J.Y., Hou, X.Z., Chu, D.D., 2022. Degradation of sulfamethazine in water by sulfite activated with zero-valent Fe-Cu bimetallic nanoparticles. J. Hazard. Mater. 431. https://doi.org/10.1016/j.jhazmat.2022.128601.
6. Fan, B., Li, X.S., Zhu, F.X., Wang, J.H., Gong, Z.M., Shao, S., Wang, X.A., Zhu, C.Y., Zhou, D.M., Gao, S.X., 2023. Anti-passivation ability of sulfidated microscale zero valent iron and its application for 1,1,2,2-tetrachloroethane degradation. J. Hazard. Mater. 443. https://doi.org/10.1016/j.jhazmat.2022.130194.
7. Fan, J.H., Liu, X., Ma, L.M., 2015. EDTA enhanced degradation of 4-bromophenol by Al^0-Fe^0-O_2 system. Chem. Eng. J. 263, 71-82. https://doi.org/10.1016/j.cej.2014.10.082.
8. Fu, F.L., Dionysios, D.D., Liu, H., 2014. The use of zero-valent iron for groundwater remediation and wastewater treatment: A review. J. Hazard. Mater. 267, 194-205. https://doi.org/10.1016/j.jhazmat.2013.12.062.
9. Gao, W.C., Zhang, Y.X., Zhang, X.Y., Duan, Z.Y., Wang, Y.H., Qin, C., Hu, X., Wang, H., Chang, S., 2015. Permeable reactive barrier of coarse sand-supported zero valent iron for the removal of 2,4-dichlorophenol in groundwater. Environ. Sci. Pollut. Res. 22, 16889-16896. https://doi.org/10.1007/s11356-015-4912-x.
10. Guo, Y.G., Zhao, Y., Yang, T.X., Gong, B., Chen. B., 2021. Highly efficient nano-Fe/Cu bimetal-loaded mesoporous silica Fe/Cu-MCM-41 for the removal of Cr(VI): Kinetics, mechanism and performance. J. Hazard. Mater. 418. https://doi.org/10.1016/j.jhazmat.2021.126344.
11. Han, C., Tang, Z.R., Liu, J.X., Jin, S.Y., Xu, Y.J., 2019. Efficient photoredox conversion of alcohol to aldehyde and H_2 by heterointerface engineering of bimetal-semiconductor hybrids. Chem. Sci. 10, 3514-3522. https://doi.org/10.1039/c8sc05813j.
12. He, F., Li, Z.J., Shi, S.S., Xu, W.Q., Sheng, H.Z., Gu, Y.W., Jiang, Y.H., Xi. B.D., 2018. Dechlorination of excess trichloroethene by bimetallic and sulfidated nanoscale Zero-Valent Iron. Environ. Sci. Technol. 52, 8627-8637. https://doi.org/10.1021/acs.est.8b01735.
13. He, N., Li, P.J., Zhou, Y.C., Ren, W.X., Fan, S.X., Verkhozina. V.A., 2009. Catalytic dechlorination of polychlorinated biphenyls in soil by palladium-iron bimetallic catalyst. J. Hazard. Mater. 164, 126-132. https://doi.org/10.1016/j.jhazmat.2008.07.149.
14. Hua, Z.C., Li, D., Wu, Z.H., Wang, D., Cui, Y.L., Huang, X.F., Fang, J.Y., An, T.C., 2021. DBP formation and toxicity alteration during UV/chlorine treatment of wastewater and the effects of ammonia and bromide. Water Res. 188. https://doi.org/10.1016/j.watres.2020.116549.
15. Huang, Y.X., Xu, H.Y., Chen, B.Y., Pan, H.M., Qiu, Z.C., 2021. Insights into chloroacetaldehydes degradation by 254 nm ultraviolet: Kinetics, products, and influencing factors. J. Environ. Chem. Eng. 9, 1. https://doi.org/10.1016/j.jece.2020.104571.
16. Ji, J.H., Xu, S.Q., Ma, Z.Q., Mou, Y.Z., 2022. Trivalent antimony removal using carbonaceous nanomaterial loaded with zero-valent bimetal (iron/copper) and their effect on seed growth. Chemosphere. 296. https://doi.org/10.1016/j.chemosphere.2022.134047.

17. Ji, Q.Q., Li, J., Xiong, Z.K., Lai, B., 2017. Enhanced reactivity of microscale Fe/Cu bimetallic particles (mFe/Cu) with persulfate (PS) for *p*-nitrophenol (PNP) removal in aqueous solution. Chemosphere. 172, 10-20. https://doi.org/10.1016/j.chemosphere.2016.12.128.
18. Li, C.H., Zhang, X.S., Wen, S.M., Xiang, R., Han, Y., Tang, W.Z., Yue, T.L., Li, Z.H., 2020. Interface engineering of zeolite imidazolate framework-8 on two-dimensional Al - metal - organic framework nanoplates enhancing performance for simultaneous capture and sensing tetracyclines. J. Hazard. Mater. 395. https://doi.org/10.1016/j.jhazmat.2020.122615.
19. Li, J., Bao, J.G., Du, J.K., Leng, Y.F., Kong, S.Q., 2018. Degradation Mechanism of Tetracycline Using Fe/Cu Oxides as Heterogeneous Activators of Peroxymonosulfate. Huanjing Kexue. 39, 3203-3211. https://doi.org/10.13227/j.hjkx.201709227.
20. Liu, X., Fan, J.H., Ma, L.M., 2015. Simultaneously degradation of 2,4-Dichlorophenol and EDTA in aqueous solution by the bimetallic Cu-Fe/O_2 system. Environ. Sci. Pollut. Res. 22, 1186-1198. https://doi.org/10.1007/s11356-014-3372-z.
21. Pan, Y., Sun, L.P., Chen, X.Y., Lin, M.Y., 2019. Removal of 2,4-dichlorophenol from groundwater by PRB simulated by CMC modified nanoscale Fe/Cu bimetal. China Environ. Sci. 39, 3789-3796. https://doi.org/10.19674/j.cnki.issn1000-6923.2019.0445.
22. Pan, Z.B., Gao, Q.Q., Chen, Z.L., 2023. Removal of As(III) and As(V) from mine groundwater using bimetallic Fe/Cu nanoparticles. Process Saf. Environ. Prot. 180, 192-204. https://doi.org/10.1016/j.psep.2023.10.014.
23. Peng, Z., Qiu, X.Y., Cai, G.Y., Zhang, X.X., Dong Z.H., 2020. Simultaneous tuning of the cation content and pore structure of cobalt-iron bimetal phosphide to enhance the electrochemical oxygen evolution. J. Alloys Compd. 842. https://doi.org/10.1016/j.jallcom.2020.155784.
24. Ren, Y., Lai, B., 2016. Comparative study on the characteristics, operational life and reactivity of Fe/Cu bimetallic particles prepared by electroless and displacement plating process. Rsc Advances, 6, 58302-58314. https://doi.org/10.1039/c6ra11255b.
25. Richardson, S.D., Plewa, M.J., Wagner, E.D., Schoeny, R., DeMarini, D.M., 2007. Occurrence, genotoxicity, and carcinogenicity of regulated and emerging disinfection by-products in drinking water: A review and roadmap for research. Mutat. Res. Rev. Mutat. Res. 636, 178-242. https://doi.org/10.1016/j.mrrev.2007.09.001.
26. Procházka, E., Melvin, S.D., Escher, B.I., Plewa, M.J., Leusch, F.D.L., 2019. Global Transcriptional Analysis of Nontransformed Human Intestinal Epithelial Cells (FHs 74 Int) after Exposure to Selected Drinking Water Disinfection By-Products. Environ. Health Perspect. 127, 11. https://doi.org/10.1289/EHP4945.
27. Ruan, X., Liu, H., Ning, X.Y., Zhao, D.Y., Fan, X.Y., 2020. Screening for the action mechanisms of Fe and Ni in the reduction of Cr (VI) by Fe/Ni nanoparticles. Sci. Total Environ. 715. https://doi.org/10.1016/j.scitotenv.2020.136822.
28. Ruan, X., Liu, H., Wang, J.W., Zhao, D.Y., Fan X.Y., 2019. A new insight into the main mechanism of 2,4-dichlorophenol dechlorination by Fe/Ni nanoparticles. Sci. Total Environ. 697.

https://doi.org/10.1016/j.scitotenv.2019.133996.

29. Sarma, K., Goswami, A., 2009. An Efficient Method for One-Pot Reductive Cleavage of Acetals to Primary Alcohols Using a Bimetal Redox Couple $CoCl_2$•$6H_2O$-Zn. Lett. Org. Chem. 6, 568-572. https://doi.org/10.2174/157017809789869456.
30. Shevchenko, G.P., Zhuravkov, V.A., Shishko, G.V., 2019. A one-pot synthesis of colloidal Ag-Au nanoparticles with controlled composition. SN Appl. Sci. 1, 1192. https://doi.org/10.1007/s42452-019-1143-7.
31. Song, H., Carraway, E.R., 2005. Reduction of chlorinated ethanes by nanosized zero-valent iron: Kinetics, pathways, and effects of reaction conditions. Environ. Sci. Technol. 39, 6237-6245. https://doi.org/10.1021/es048262e.
32. Song, S.W., Wang, Y.H, Tian, P.F., Zang, J.B., 2022. One-step complexation and self-template strategy to synthesis bimetal Fe/Mn-N doped interconnected hierarchical porous carbon for enhancing catalytic oxygen reduction reaction. Int. J. Hydrogen Energy. 47, 24728-24737. https://doi.org/10.1016/j.ijhydene.2022.05.218.
33. Sun, L., Song, H.O., Li, Q., Li. A.M., 2016. Fe/Cu bimetallic catalysis for reductive degradation of nitrobenzene under oxic conditions. Chem. Eng. J. 283, 366-374. https://doi.org/10.1016/j.cej.2015.06.065.
34. Tian, X.M., Shen, Z.Q., Zhou, Y.X., Wang, K.J., 2021. Acidification inhibition, biodechlorination, and biotransformation of chlorinated acetaldehydes on acidogenic sludge and microbial community changes. Chemosphere. 277. https://doi.org/10.1016/j.chemosphere.2021.130231.
35. Tian, X.M., Song, Y.D., Xi, H.B., Shen, Z.Q., Zhou, Y.X., Wang, K.J., 2020. Inhibition and removal of trichloroacetaldehyde by biological acidification with glucose co-metabolism. J. Hazard. Mater. 386. https://doi.org/10.1016/j.jhazmat.2019.121796.
36. Wei, Z.Y., Li, X.Q., Han, S., Yan, C.H., Sun, M.C., Liu, Y., Fan, L., 2022. Effective and selective conversion of nitrate from aqueous solutions to nitrogen gas under neutral pH condition using Al/Cu bimetal-sulfamic acid reduction method. Sep. Purif. Technol. 287. https://doi.org/10.1016/j.seppur.2022.120618.
37. Yamaguchi, R., Kurosu, S., Suzuki, M., Kawase, Y., 2018. Hydroxyl radical generation by zero-valent iron/Cu (ZVI/Cu) bimetallic catalyst in wastewater treatment: Heterogeneous Fenton/Fenton-like reactions by Fenton reagents formed in-situ under oxic conditions. Chem. Eng. J. 334, 1537-49. https://doi.org/10.1016/j.cej.2017.10.154.
38. Yang, B., Zhang, J.X., Zhang, Y.F., Deng, S.B., Yu, G., Wu, J.H., Zhang, H., Liu, J.H., 2014. Promoting effect of EDTA on catalytic activity of highly stable Al-Ni bimetal alloy for dechlorination of 2-chlorophenol. Chem. Eng. J. 250, 222-29. https://doi.org/10.1016/j.cej.2014.04.014.
39. Yang, W.C., Xi, D.D., Li, C.F., Yang, Z.H., Lin, Z., Si, M.Y., 2021. "In-situ synthesized" iron-based bimetal promotes efficient removal of Cr(VI) in by zero-valent iron-loaded hydroxyapatite. J. Hazard. Mater. 420. https://doi.org/10.1016/j.jhazmat.2021.126540.

40. Yu, X.M., Zhao, S.Y., Yuan, S.J., Wang, W., Hu, Z.H., 2020. Formation potential of halogenated aldehydes and ketones disinfection by-products and structural characteristics of their precursors. Huanjing Huaxue. 39, 28-38. https://doi.org/10.7524/j.issn.0254-6108.2019012602.
41. Yuan, Y., Li, H.Q., Lai, B., Yang, P., Gou, M., Zhou, Y.X., Sun, G.Z., 2014. Removal of High-Concentration CI Acid Orange 7 from Aqueous Solution by Zerovalent Iron/Copper (Fe/Cu) Bimetallic Particles. Ind. Eng. Chem. Res. 53, 2605-2613. https://doi.org/10.1021/ie402739s.
42. Zeng, Y.B., Walker, H, Zhu, Q.Z., 2017. Reduction of nitrate by NaY zeolite supported Fe, Cu/Fe and Mn/Fe nanoparticles. J. Hazard. Mater. 324, 605-16. https://doi.org/10.1016/j.jhazmat.2016.11.032.
43. Zhang, S.H., You, J.P., An, N., Zhao, J.K., Wang, L.D., Cheng, Z.W., Ye, J.X., Chen, D.Z., Chen, J.M., 2018. Gaseous toluene powered microbial fuel cell: Performance, microbial community, and electron transfer pathway. Chem. Eng. J. 351, 515-522. https://doi.org/10.1016/j.cej.2018.06.027.
44. Zhang, W., Li, L., Li, B.Z., Lin, K.F., Lu, S.G., Fu, R.B., Zhu, J., Cui, X.H., 2013. Mechanism and Pathway of Tetrachloroethylene Dechlorination by Zero-Valent Iron with Cu or Cu/C, J. Environ. Eng. 139, 803-809. https://doi.org/10.1061/(ASCE)EE.1943-7870.0000693.
45. Zhao, X., Liu, W., Cai, Z.Q., Han, B., Qian, T.W., Zhao, D.Y., 2016. An overview of preparation and applications of stabilized zero-valent iron nanoparticles for soil and groundwater remediation. Water Res. 100, 245-266. https://doi.org/10.1016/j.watres.2016.05.019.
46. Zhou, C.L., Zhou, Y.Q., Jiang, J.Y., Xie, Z., Wang, Z.Y., Zhang, J.H., Wu, J.H., Yin, H., 2004. Organometallic reactions in aqueous media:: the allylations of carbonyl compounds mediated in $Zn/CdSO_4$ and $Zn/SnCl_2$ bimetal systems. Tetrahedron Lett. 45, 5537-5540. https://doi.org/10.1016/j.tetlet.2004.05.070.
47. Zhou, T., Huang, Y., Zhang, J.F., Hu, M.T., 2023. The origin of highly efficient and selective activated carbon supported bimetallic Fe@Cu composite for Fe(II)EDTA-NO reduction in Fe(II)EDTA complexation denitrification process. Fuel. 333. https://doi.org/10.1016/j.fuel.2022.126561.
48. Zhu, L., Lin, H.Z., Qi, J.Q., Xu, X.Y., Qi, H.Y., 2012. Effect of H_2 on reductive transformation of *p*-ClNB in a combined ZVI-anaerobic sludge system. Water Res. 46, 6291-6299. https://doi.org/10.1016/j.watres.2012.08.029.
49. Zhu, N.R., Luan, H.W., Yuan, S.H., Chen, J., Wu, X.H., Wang, L.L., 2010. Effective dechlorination of HCB by nanoscale Cu/Fe particles, J. Hazard. Mater. 176, 1101-1105. https://doi.org/10.1016/j.jhazmat.2009.11.092.

Figures

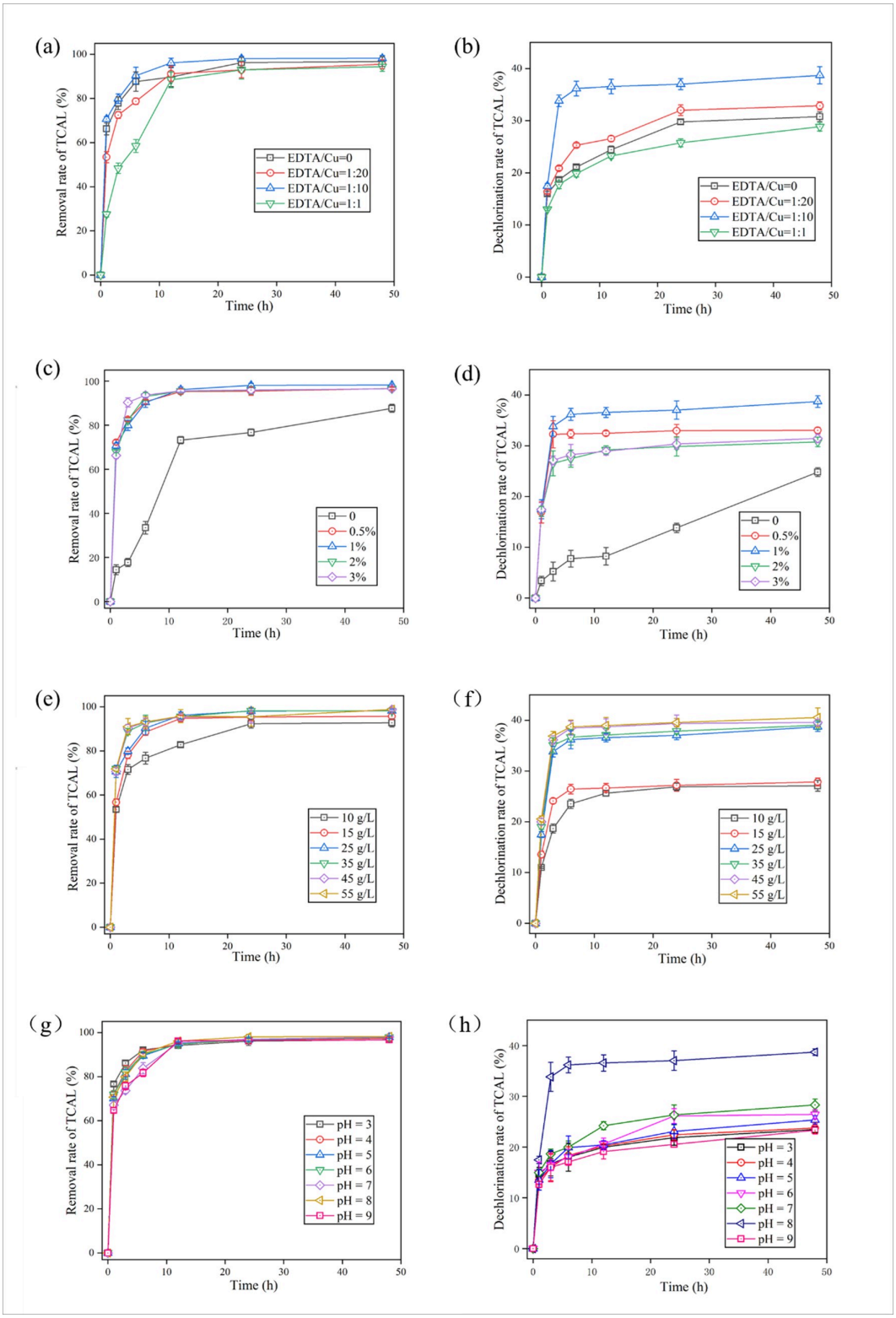


Figure 1

Removal and dechlorination of TCAL by Fe/Cu bimetallic particles under various conditions. (a, b) Effects of EDTA proportions. (c, d) Effects of copper loads. (e, f) Effects of particle dosages. (g, h) Effects of initial pH values.

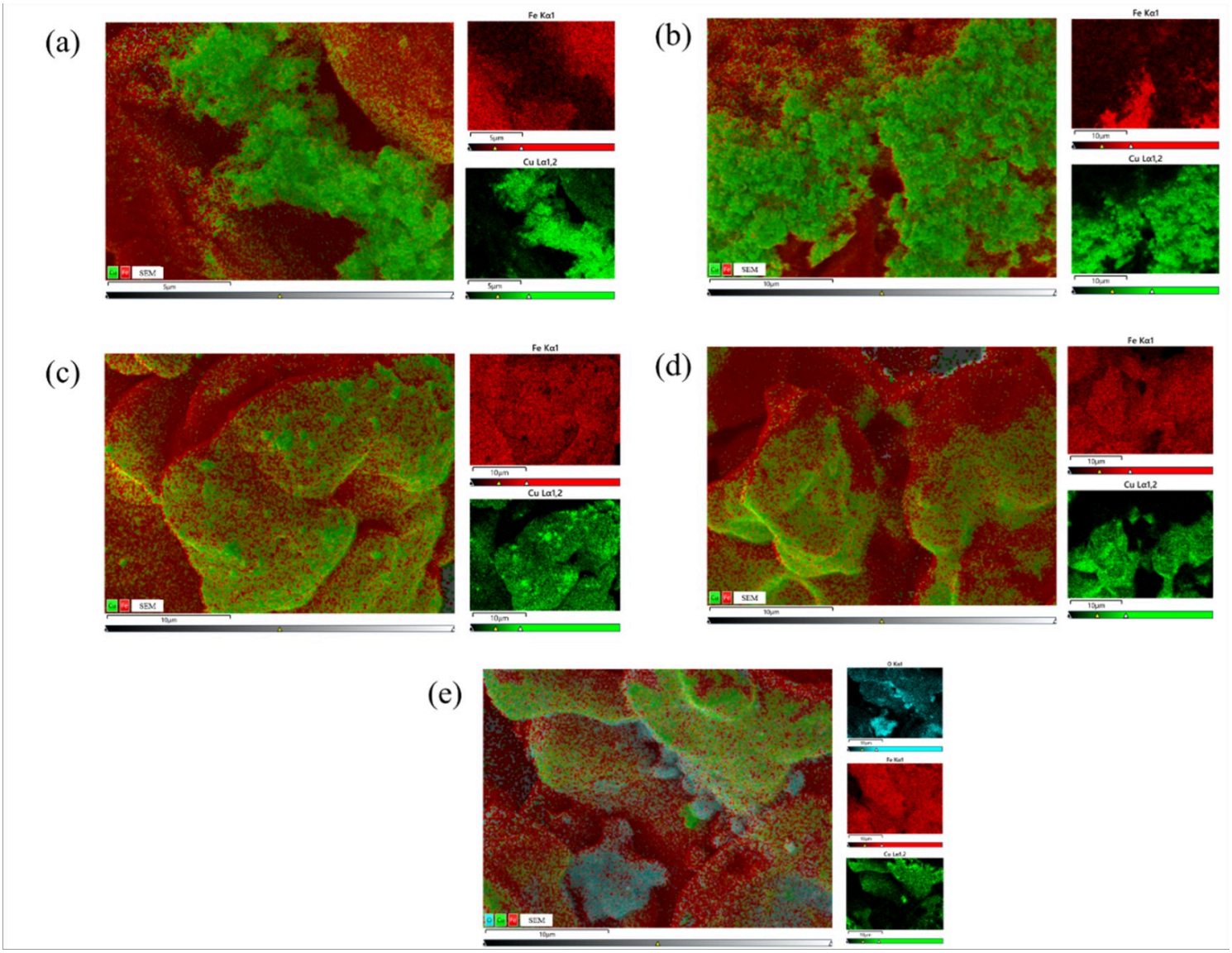


Figure 2

SEM-EDS images of Fe/Cu with different dosages of EDTA ((a) EDTA/Cu = 0; (b) EDTA/Cu = 1/20; (c) EDTA/Cu = 1/10; (d) EDTA/Cu = 1/1) and after (e) the use of Fe/Cu with EDTA/Cu = 1/10

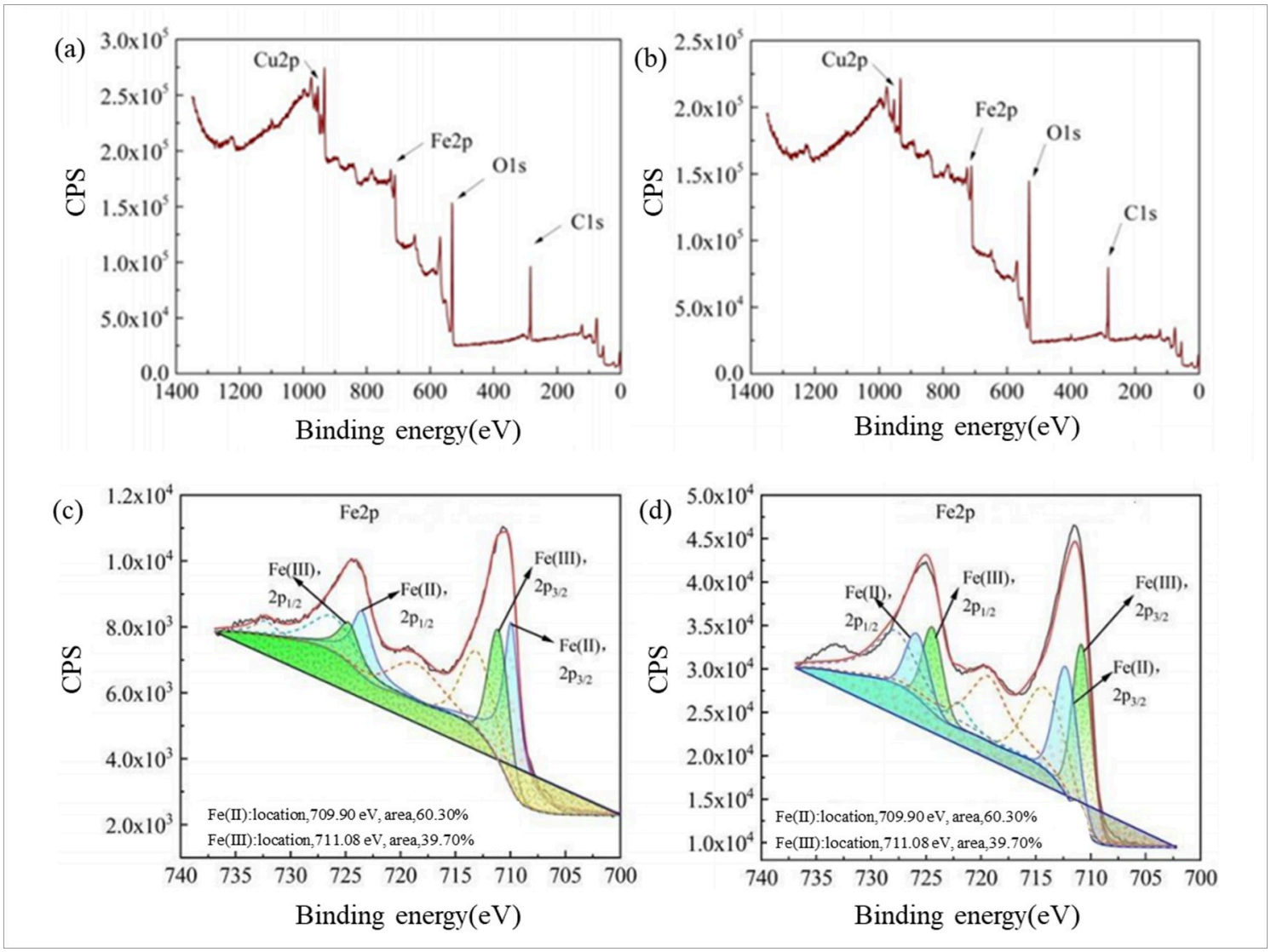


Figure 3

XPS images of Fe/Cu before (a, c) and after (b, d) the use

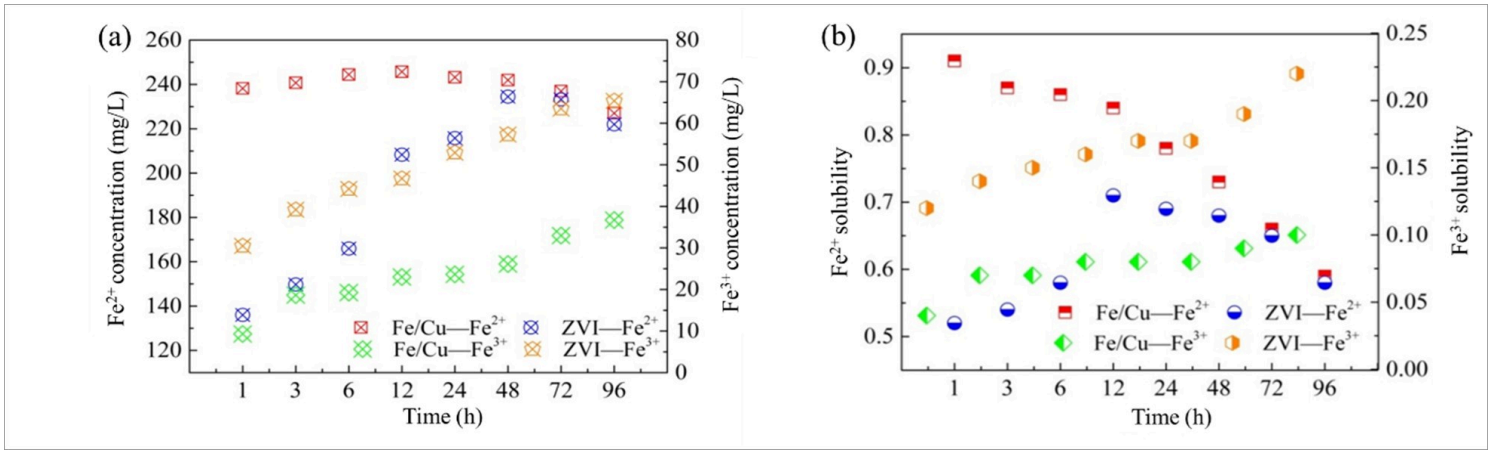


Figure 4

The concentrations (a) and solubility (b) of Fe^{2+} and Fe^{3+} during dechlorination in reduction of TCAL by ZVI and Fe/Cu

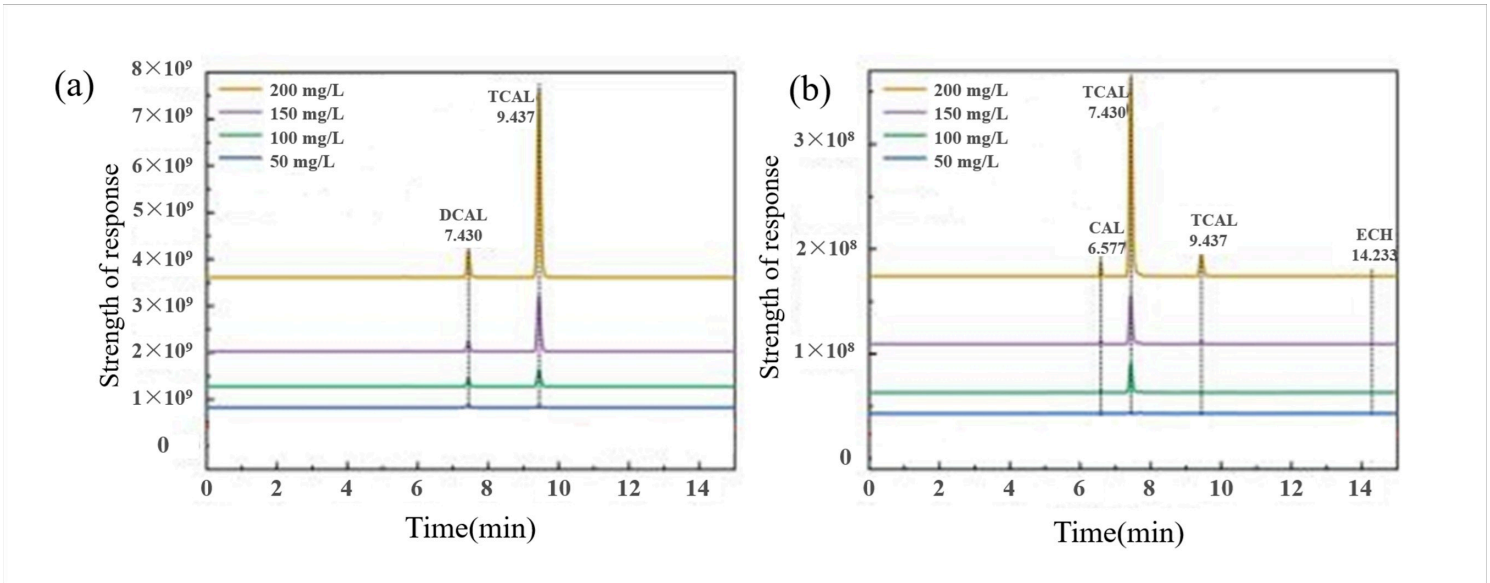


Figure 5

GC-μECD of products during reductive dechlorination of TCAL by Fe/Cu bimetallic particles at 6 h (a) and 96 h (b)

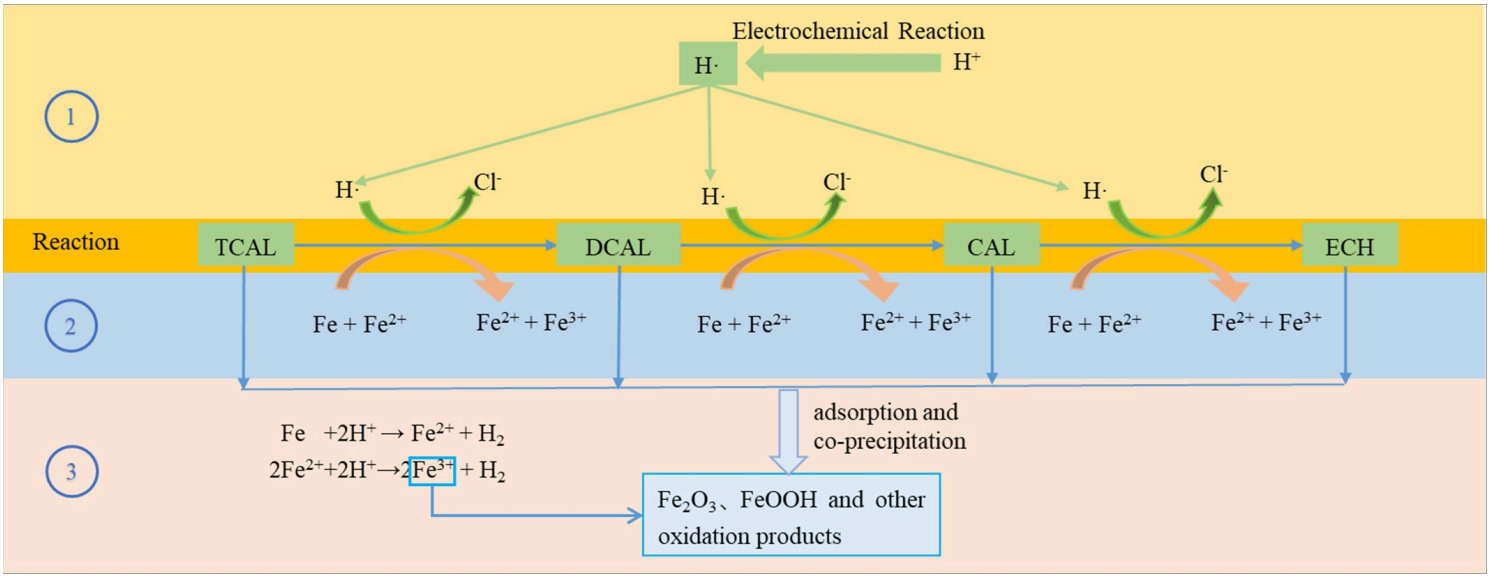


Figure 6

Mechanism of TCAL removal via reduction and adsorption by Fe/Cu system

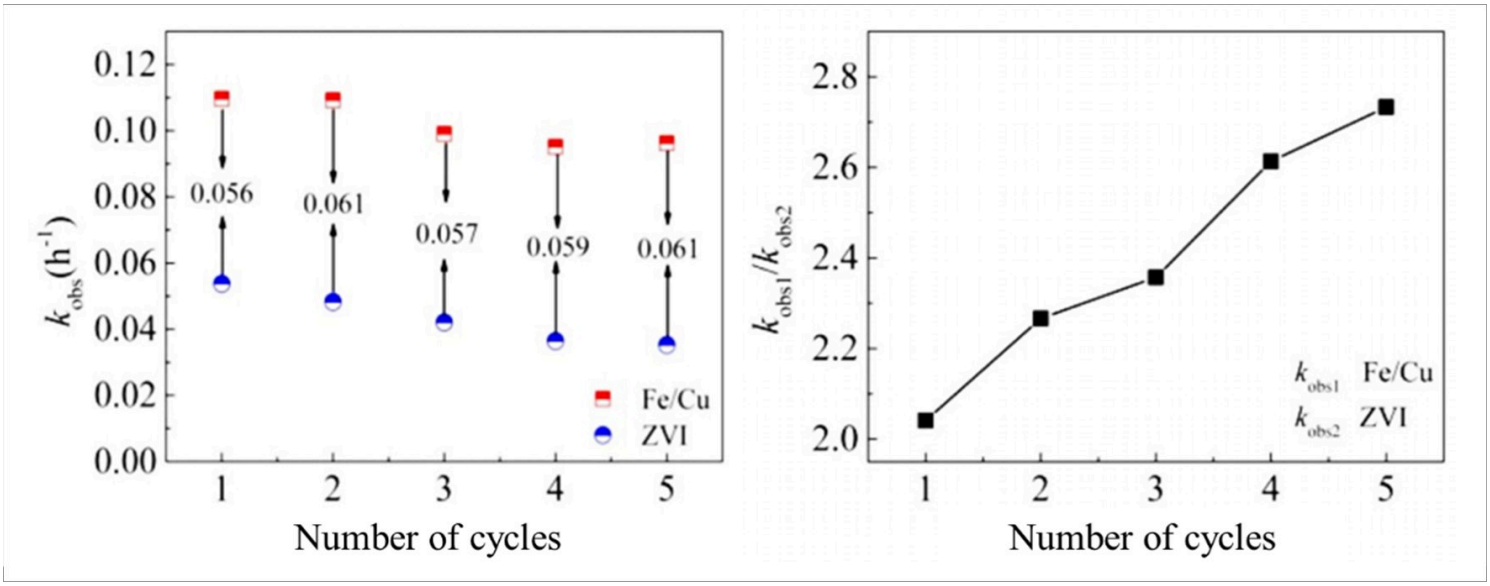


Figure 7

Reusability of Fe/Cu and ZVI in TCAL removal cycles

Supplementary Files

This is a list of supplementary files associated with this preprint. Click to download.

- SupplementaryMaterial.docx